Analysis and Experimental Verification of the Moving-Magnet Linear Actuator with Cylindrical Halbach and Radial Array

Seok-Myeong Jang*, Jang-Young Choi*, Sung-Ho Lee**, Han-Wook Cho* and Won-Bum Jang*

Abstract - In the machine tool industry, direct drive linear motor technology is of increasing interest as a means to achieve high acceleration and to increase reliability. This paper analyzes and compares the characteristics of the tubular linear actuator with the cylindrical Halbach and radial array, respectively. A tubular linear actuator with cylindrical Halbach array, consisting of parallel magnetized arc segments instead of ideal radial and axial magnetized rings, is manufactured. The magnetic field solutions due to the PMs and to the currents are established analytically in terms of vector potential, using the 2-D cylindrical coordinate system. Motor thrust, flux linkage and back emf are then derived. Thrust characteristics according to such design parameters as magnet height and air gap length are also given. The results are validated extensively by comparison with finite element analysis (FEA). Test results such as thrust measurements are also given to confirm the analysis.

Keywords: Cylindrical Halbach array, tubular linear actuator, parallel magnetized arc segments.

1. Introduction

Our work is motivated by the desire to develop a direct drive linear actuator for machine tool applications. Recently, many linear motion motors are rapidly finding applications that range from short stroke linear motion vibrators, such as compressors and textile machines [1]. The advantages of such a motor are that it has good linearity and can be used without mechanical energy conversion parts, which change rotary motion into linear motion, such as screws, gears, chains, and so on. Moreover, tubular structures are very attractive compared with flat linear actuators, owing to the absence of end-turn effects and high thrust. So, despite such disadvantages of the tubular linear actuator as difficulty in manufacturing a permanent magnet mover and maintaining fixed air gap length, among various linear machine configurations, tubular machines with permanent magnet excitation become an attractive candidate for applications in which dynamic performance and reliability are crucial [2].

In this paper, tubular linear actuators with cylindrical Halbach array and tubular linear actuators with radial array are analyzed, with reference to the following parameters as variables: magnetic field, flux linkage, motor thrust and back emf. These variables are derived using an analytical method known as the 2-D cylindrical coordinate system. The results are validated extensively by comparison with the finite element method. Finally, a tubular linear actuator with cylindrical Halbach array composed of parallel magnetized arc segments is manufactured and the experimental results prove the validity of the analytical results.

* Department of Electrical Engineering, Chungnam National University, Daejeon, 305-764, Korea. (smjang@ee.cnu.ac.kr, aramis76@cnu.ac.kr, hwcho@cnu.ac.kr, wbjang@hanafos.com)
** LG Digital Appliance Lab., 327-23, Gasandong, Gumchun-gu, Seoul, Korea. (iemechas@lge.com and shlee@ee.cnu.ac.kr).
Received: October 2, 2003 ; Accepted: November 3, 2003

2. Tubular structures and analytical model

Fig. 1 shows the schematic of the tubular linear actuator. Fig. 2 shows the cross section, excluding stator windings, of the tubular linear actuator sketched in Fig. 1. Analyzing the magnetic fields due to PMs, we regard the winding region as the air region. Consequently, the magnetic field analysis is confined to two regions. Roman numerals I and II in Fig. 2 represent the air region and the magnet region, respectively. Therefore,

$$B = \begin{cases} \mu_0 H & \text{in the air/stator windings} \\ \mu_0 \mu_r H + \mu_0 M & \text{in the magnets} \end{cases} \quad (1)$$

where μ_r is the relative recoil permeability of the magnets and assumed unity, that is, μ_r =1. M is the remanent magnetization. Fig. 3 (a) and (b) details the single and three phase current density distribution, respectively. We assume that the stator current flows through an infinitesimally thin sheet on the interior surface of the stator, at $r=r_s$. This paper also assumes that both iron permeability and motor length are infinite.

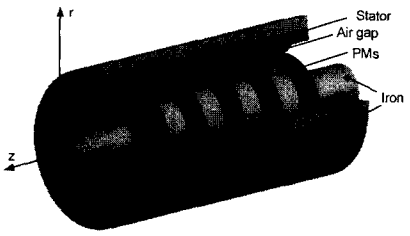

Fig. 1 Schematic of tubular linear actuator

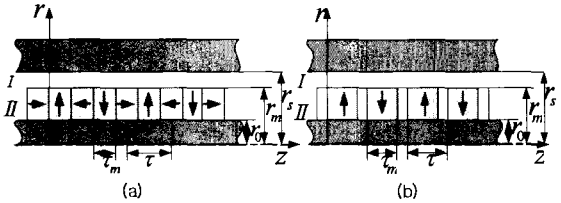

Fig. 2 Cross section of the tubular linear actuator with cylindrical Halbach array (a) and radial array (b)

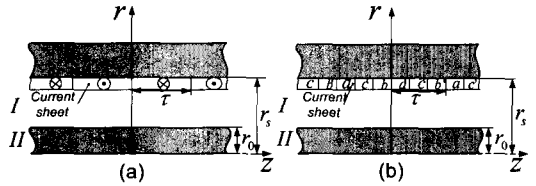

Fig. 3 Single-phase (a) and three-phase (b) current density distribution

3. Magnetic fields due to the PMs

3.1 Governing Equations

Since there is no free current in the magnetic region, curl$H$=0. Therefore, $\nabla\times B=\mu_0\nabla\times M$. The magnetic vector potential A is defined as $\nabla\times A=B$. By the geometry of the tubular linear actuator, the vector potential has only θ-components. Therefore, the Poisson's equation for cylindrical Halbach and radial array is given by:

$$\frac{\partial^2}{\partial r^2}A_\theta+\frac{1}{r}\frac{\partial}{\partial r}A_\theta-\left(k_n^2+\frac{1}{r^2}\right)A_\theta=-\mu_0 k_n\left(\frac{c_1}{r}+c_2 r\right)M_{rn} \quad (2)$$

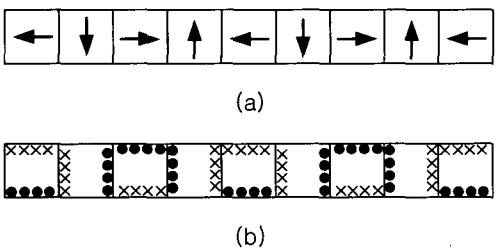

Fig. 4 Dual electro magnetization of cylindrical Halbach array: (a) Halbach magnet array (b) Equivalent current model.

where the pole pitch of the actuator is τ, and the spatial wave number of the nth harmonic is $k_n = n\pi/\tau$.. Here M_{rn} is the Fourier coefficient of nth-order radial magnetization components in radial and Halbach array. The coefficients c_1 and c_2 are appropriately selected to reduce the modification of radial component M_r in magnetization M [3].

3.2 Boundary Conditions

Halbach magnet array in Fig. 4 (a) can be expressed as an equivalent current model by applying Ampere's law in Fig. 4 (b). As such, in the case of boundary conditions for Halbach array, the equivalent current, which is due to axial components in Halbach array and distributed in the upper and lower surface of the permanent magnet must be considered. As a result, boundary conditions of the tubular linear actuator with cylindrical Halbach and radial array in Fig. 2 are given by:

Cylindrical Halbach array model

$$\begin{aligned} &B_z^{II}(r_o,z)=-\mu_0 M_{zn}\\ &B_r^{II}(r_m,z)=B_r^{I}(r_m,z)\\ &B_z^{II}(r_m,z)-B_z^{I}(r_m,z)=-\mu_0 M_{zn}\\ &B_z^{I}(r_s,z)=0 \end{aligned} \quad (3.a)$$

Radial array model

$$\begin{aligned} &B_z^{II}(r_o,z)=0\\ &B_r^{II}(r_m,z)=B_r^{I}(r_m,z)\\ &B_z^{II}(r_m,z)=B_z^{I}(r_m,z)\\ &B_z^{I}(r_s,z)=0 \end{aligned} \quad (3.b)$$

where M_{zn} is the Fourier coefficient of n*th*-order axial magnetization components in cylindrical Halbach array.

3.3 Characteristic Equations for Flux Density

The resulting axial and radial components of flux density are given by:

$$\begin{aligned} B_{zn}^{I}&=k_n[A_n^{I}I_0(k_n r)-B_n^{I}K_0(k_n r)]\cos(k_n z)\\ B_{zn}^{II}&=k_n[A_n^{II}I_0(k_n r)-B_n^{II}K_0(k_n r)+\frac{2c_2\mu_0 M_{rn}}{k_n^2}]\cos(k_n z)\\ B_{rn}^{I}&=k_n[A_n^{I}I_1(k_n r)+B_n^{I}K_1(k_n r)]\sin(k_n z)\\ B_{rn}^{II}&=k_n[A_n^{II}I_1(k_n r)+B_n^{II}K_1(k_n r)+\frac{\mu_0 M_{rn}}{k_n}\left(\frac{c_1}{r}+c_2 r\right)]\sin(k_n z) \end{aligned} \quad (4)$$

where I_1 and K_1 are modified Bessel functions of the first and second kind of order one, and I_0 and K_0 are modified Bessel functions of the first and second kind of order zero

[4] Equation (4) can be applied to both the tubular linear actuator model with cylindrical Halbach and the radial array; the coefficients A_n^I, B_n^I, A_n^{II} and B_n^{II} are only different in each model. These coefficients are determined by substituting (3) for (4).

4. Magnetic fields due to the stator currents

The linear current density J may be expanded into a Fourier series, via

$$J_\theta(z) = \sum_{n=1,odd}^{\infty} J_n \sin(k_n z) \tag{5}$$

where J_n is the function of the current value and the winding distribution. Since this paper assumes that the current is distributed in an infinitesimal thin sheet, both air/stator windings and iron regions remain characterized by curl$H$=0 and then magnetic fields are computed by means of the vector potential. Governing equation is represented by Laplace's equation (2), with M_{rn}=0. The boundary conditions are given by:

$$\begin{aligned} B_z^I(r_s,z) &= \mu_0 J_\theta(z) \\ \mu_r B_z^I(r_o,z) &= B_z^{II}(r_o,z) \\ B_r^{II}(r_o,z) &= B_r^I(r_o,z) \end{aligned} \tag{6}$$

where μ_r is the relative recoil permeability of the iron with supposed infinity, that is, $\mu_r = \infty$.

The resulting characteristic equations of flux density are given by:

$$\begin{aligned} B_{rn}^I &= \mu_0 k_n [-I_1(k_n r) + \chi_n k_1(k_n r)] \upsilon_n J_n \cos(k_n z) \\ B_{zn}^I &= \mu_0 k_n [I_0(k_n r) + \chi_n k_0(k_n r)] \upsilon_n J_n \sin(k_n z) \end{aligned} \tag{7}$$

where the coefficients χ_n, υ_n are given by

$$\upsilon_n = \frac{1}{k_n[I_0(k_n r_s) + \chi_n K_0(k_n r_s)]} \quad \chi_n = -\frac{I_0(k_n r_o)}{K_0(k_n r_o)}$$

5. The flux linkages, back emf and thrust force

The flux linkage of each phase is given by:

$$\lambda = \int_i^f \frac{N}{\tau} \int_z^{z+\tau} 2\pi r_s B_r(z) dz dz \tag{8}$$

where N is the number of conductors per pole, and i and f are the initial and final position of the considered phase respectively.

The back electromotive force of each phase is given by: [5]

$$e_b = \frac{d\lambda}{dt} = \frac{dz}{dt}\frac{d\lambda}{dz} = v\frac{d\lambda}{dz} \tag{9}$$

Thus, back emf is given by the product of velocity v and the rate of change in flux linkage with respect to position.

The axial thrust exerted on the stator winding results from the interaction between the current density and the permanent magnet field. In the general position z, the thrust in an infinitesimal tubular motor length dz is given by:

$$dF_z(z) = -2\pi r_s J_\theta(z) B_r^I(r_s, z) dz \tag{10}$$

It has the advantage that (10) is free from integrals of Bessel functions related to formula $F = \int_v (J \times B) dv$, that cause a significant analytical burden.

Table 1 Specifications of tubular linear actuator used in comparison of analytical and FEA

Parameters	Tubular linear actuator with radial magnetized PMs mover	Tubular linear actuator with radial magnetized PMs mover
T	20(mm)	
τ_m	15(mm)	10(mm)
r_o	10(mm)	
r_m	20(mm)	
r_s	25(mm)	
Remanence	1.1 (T)	
Pole number	4	4 and 1/2

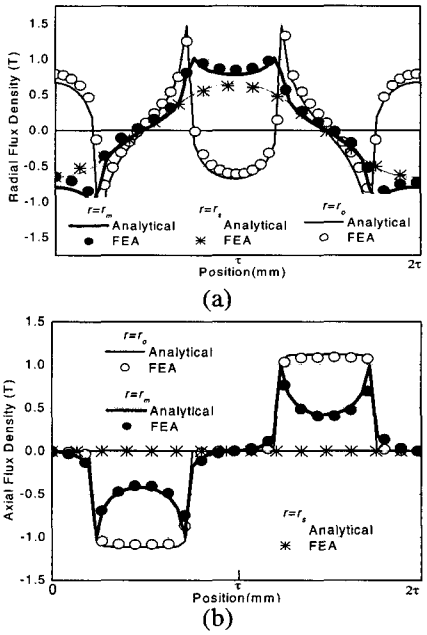

Fig. 5 Radial (a) and axial (b) flux density distributions for the tubular Halbach array topology

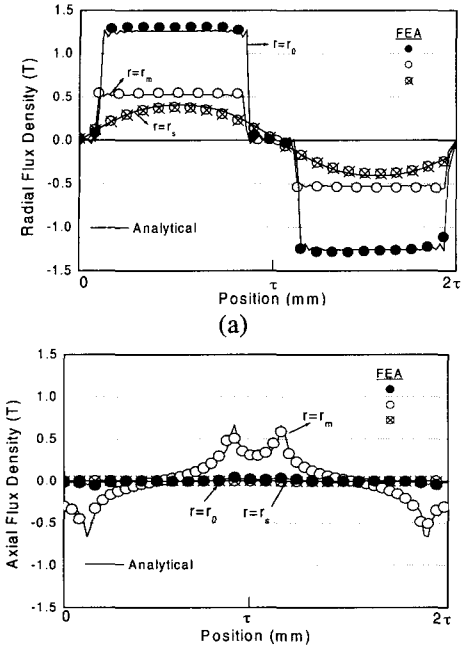

(a)

(b)

Fig. 6 Radial (a) and axial (b) flux density distributions for the tubular radial array topology

6. Comparison of analytical and FE results

The results of the analytical model have been compared with those obtained by a FE model. The specifications of the tubular linear actuator are presented in Table 1.

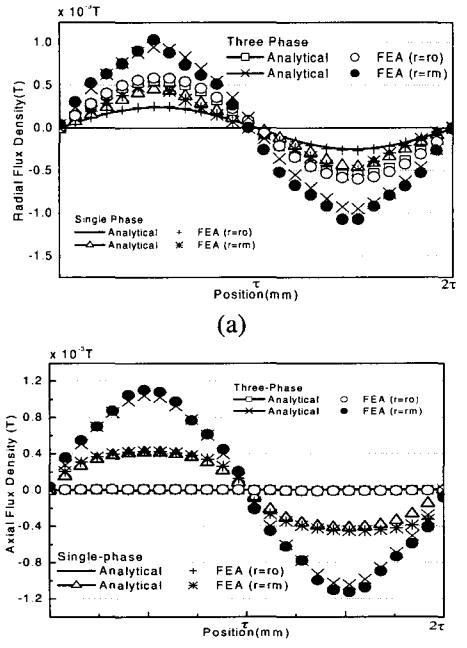

(a)

(b)

Fig. 7 Radial (a) and axial (b) flux density distributions due to single- and three-phase currents

6.1 Magnetic Fields due to PMs

Figs. 5 and 6 show the comparison of analytical and FE results of both radial and axial flux density distributions for tubular cylindrical Halbach array and radial array topology, respectively. The results are shown to be in good agreement with those obtained from FEA.

6.2 Magnetic Fields due to the Stator Windings

Fig. 7 (a) and (b) shows the radial and axial flux density distributions due to the single- and three-phase currents, respectively. In the case of single-phase windings, turns per pole are 10 turns and a coil current is 1(A) and then, in case of three-phase windings, turns per pole per phase are 5 turns and the three-phase currents are i_a =2(A), i_b = i_c = -1(A).

6.3 Flux Linkages and Back EMF

Figs. 8 and 9 show the flux linkage and back EMF for the tubular linear actuator with two different array patterns respectively. It can be seen that the analytical results are in better agreement with those obtained from FEA in three-phase windings than those in single-phase windings. Especially, in case of mover velocity v=100(*mm/s*), the analytical results of back EMF are compared with FE results.

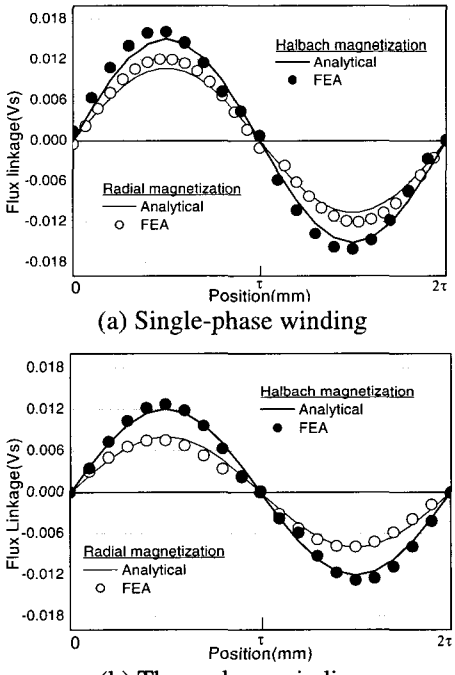

(a) Single-phase winding

(b) Three-phase winding

Fig. 8 Flux linkage for the tubular linear actuator with two different array patterns

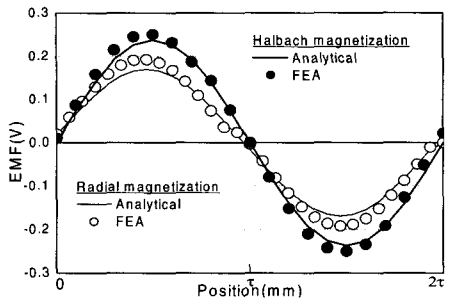

(a) Single-phase winding

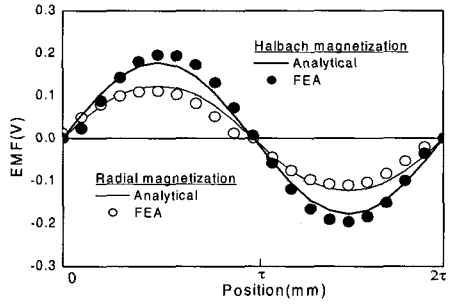

(b) Three-phase winding

Fig. 9 Back-emf for the tubular linear actuator with two different array patterns

6.4 Thrust force

Fig. 10 shows the comparison between analytical and FE results of axial thrust according to mover position for the tubular linear actuator with two different array patterns. It can be seen that thrust of the tubular linear actuator with cylindrical Halbach array is superior to that with radial array.

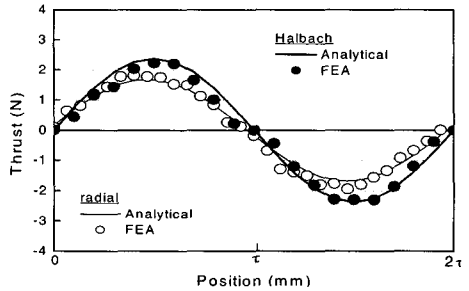

(a) Single-phase winding

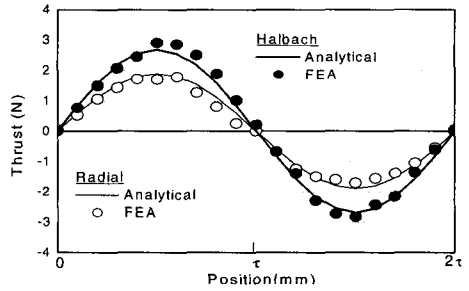

(b) three-phase winding

Fig. 10 Thrust vs. mover position for the tubular linear actuator with two different array patterns

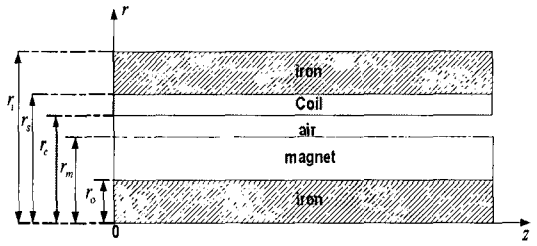

Fig. 11 Tubular linear actuator model for thrust analysis according to design parameters

7. Thrust characteristics according to design parameters

Fig. 11 shows a tubular linear actuator analytical model for thrust analysis according to design parameters. The fixed design parameters for thrust analysis according to air-gap length and magnet height are given in Tables II and III, respectively.

7.1 Thrust Characteristics according to Air Gap Length

For a fixed pole pitch τ , Figs. 12 and 13 show Peak thrust variations acting on the cylindrical Halbach array mover and the radial array mover vs. $(r_c-r_m)/\tau$ for various values of r_m/τ respectively, in case of single-phase winding with i=2 (A) and three-phase winding with i_a =2(A), $i_b = i_c$ = -1(A).

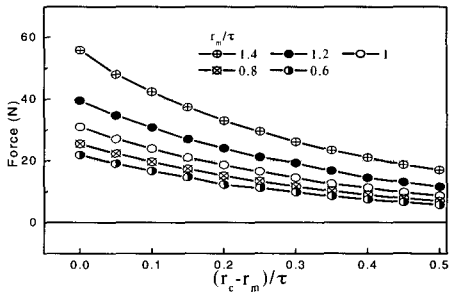

(a)

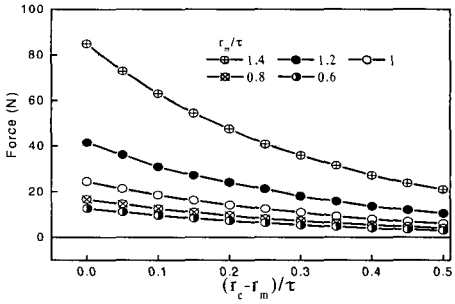

(b)

Fig. 12 Peak thrust acting on the Halbach array mover vs. $(r_c-r_m)/\tau$ for various values of r_m/τ: single-phase winding with i=2(A) (a) and three-phase winding with i_a =2(A), $i_b = i_c$ = -1(A) (b)

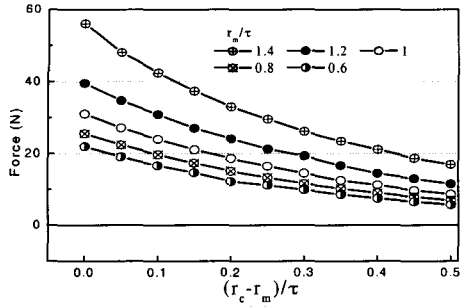

(a)

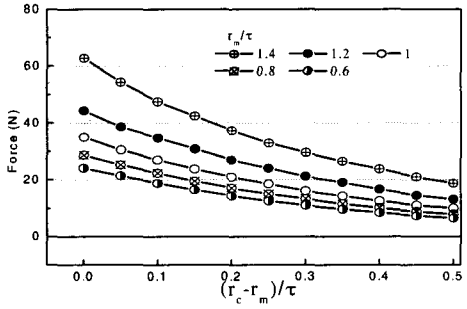

(b)

Fig. 13 Peak thrust acting on the radial array mover vs. $(r_c-r_m)/\tau$ for various values of r_m/τ: single-phase winding with i=2(A) (a) and three-phase winding with i_a =2(A), $i_b = i_c$ = -1(A) (b)

It can be seen that the greater the air gap length, that is the more $(r_c-r_m)/\tau$ increases, the more peak thrust decreases as an exponential function and the more magnet height, that is the more r_m/τ decreases, the more peak thrust variations are slowed down. When comparing Fig. 12 with Fig. 13, the thrust characteristics of the Halbach array model are superior to those of the radial array model.

7.2 Thrust Characteristics according to Magnet Height

For a fixed air-gap length r_c-r_m, Figs. 14 and 15 show that Peak thrust variations acting on the Halbach array mover and the radial array mover vs. $(r_m-r_o)/(r_c-r_m)$ for various values of $\tau/(r_c-r_m)$ respectively, in case of single-phase winding with i=2(A) and three-phase winding with i_a =2(A), $i_b = i_c$ = -1(A). It can be seen that the greater the magnet height, that is the more r_m-r_o /r_c-r_m increases, the more peak thrust increases nonlinearly and the greater the pole pitch, that is $\tau/(r_c-r_m)$ increases, the more the differences in peak thrust variations are slowed down. Especially, in the case of the Halbach array model, the greater the pole pitch, the more the thrust increases by the value of $\tau/(r_c-r_m)$ up to 10, but thrust time of the value of $\tau/(r_c-r_m)$ equals 20 is lower than the time of the value of $\tau/(r_c-r_m)$ equals 10, as shown in Fig. 13. Therefore, for a fixed air-gap length, optimum magnet height and pole pitch can be determined for PMs to be utilized efficiently from these results.

Table 2 Fixed design parameters for thrust analysis according to air-gap length

Parameters	Radial-1phase	Radial-3phase	Halbach-1phase	Halbach-3phase
T	20(mm)			
τ_m	15(mm)		10(mm)	
r_o	10(mm)			
r_s-r_c	5(mm)			
r_i-r_s	10(mm)			

Table 3 Fixed design parameters for thrust analysis according to magnet height

Parameters	Radial-1phase	Radial-3phase	Halbach-1phase	Halbach-3phase
r_c-r_m	4(mm)			
r_o	10(mm)			
r_s-r_c	4(mm)			
r_i-r_s	10(mm)			

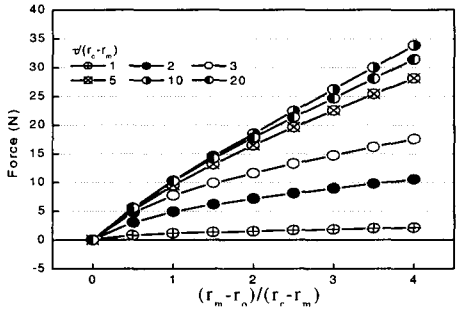

(a)

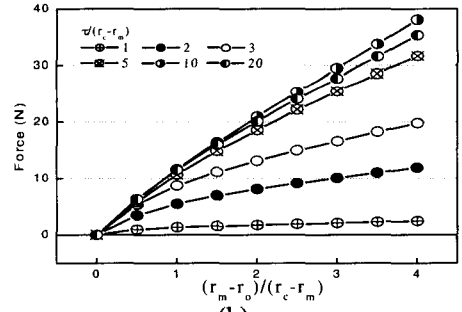

(b)

Fig. 14 Peak thrust acting on the Halbach array vs. $(r_m-r_o)/(r_c-r_m)$ for various values of $\tau/(r_c-r_m)$: single-phase winding with i=2(A) (a) and three-phase winding with i_a =2(A), $i_b = i_c$ = -1(A) (b)

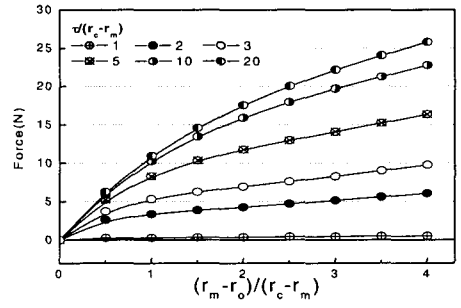

(a)

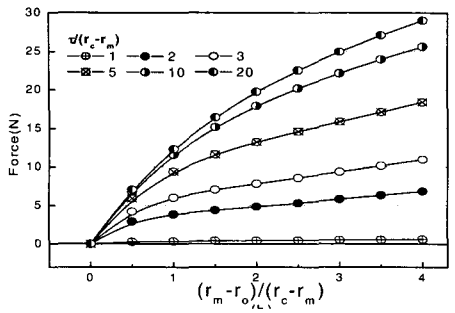

(b)

Fig. 15 Peak thrust acting on the Halbach array vs. $(r_m-r_o)/(r_c-r_m)$ for various values of $\tau/(r_c-r_m)$: single-phase winding with i=2(A) (a) and three-phase winding with i_a =2(A), $i_b = i_c$ = -1(A) (b)

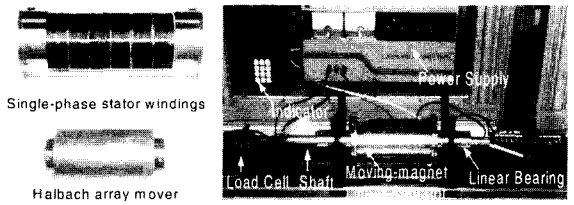

(a) (b)

Fig. 16 Photograph of the tubular linear actuator with Halbach array mover: single-phase stator winding and Halbach array mover (a) and testing apparatus (b)

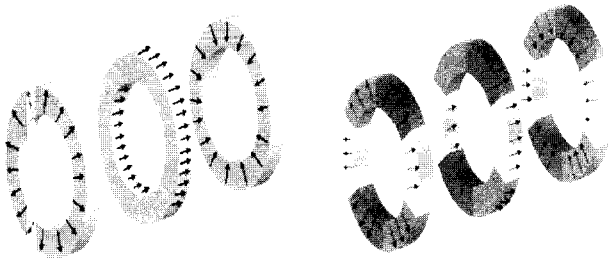

(a) (b)

Fig 17 Halbach arrays with the ideal radial magnetized ring (a) and parallel magnetized arc segments (b)

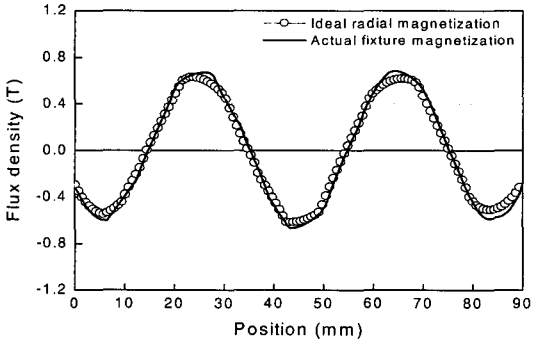

Fig. 18 Comparison of predicted radial component of flux density at the air-gap for both ideal radial magnetization and actual fixture magnetization

8. Manufacture and thrust measurement

8.1 Manufactured Model and Experimental Systems

Fig. 16 (a) displays a photograph of the cylindrical Halbach array mover and single-phase stator windings. Fig. 16 (b) shows the experimental system consisting of load cell, indicator, DC power supply and tubular linear actuator with cylindrical Halbach array to measure static thrust. Specifications of manufactured tubular linear actuator are presented in Table 4.

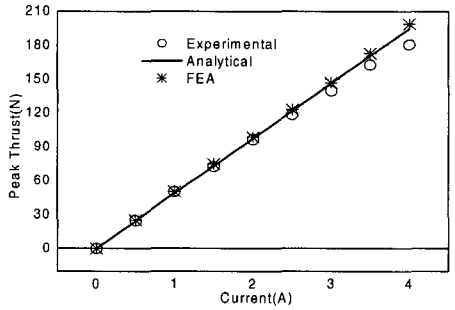

Fig. 19 Thrust vs. coil current for the tubular linear actuator with Halbach array mover

Table 4 Specifications of the manufactured tubular actuator with Halbach array

Halbach array mover		Stator windings	
Parameter (symbol)	Value (unit)	Parameter (symbol)	Value (unit)
Shaft radius (r_o)	20 (mm)	Stator winding inner radius (r_c)	31(mm)
PM outer radius (r_m)	30 (mm)		
Pole pitch (τ)	20 (mm)	Stator winding outer radius (r_s)	35(mm)
PM pole pitch (τ_m)	10 (mm)		
Pole number (P)	4and1/2	Stator outer radius (r_i)	45(mm)
Mover length (l)	90 (mm)	Turns	100

8.2 Characteristic of Flux Density

Fig. 17 (a) presents that a cylindrical Halbach array consists of ideal radial magnetized ring and ideal axial magnetized ring. In the case of a ring magnet, a geometry-specific impulse magnetizing fixture is required to impart the magnetization, whereas arc segments can be magnetized with a parallel magnetization such as in Fig. 17 (b) [6]. So, this paper introduces parallel magnetized arc segments as a mover, which offers advantages not only in reducing the burden in the manufacture of ideal radial magnetized PMs, but also in cutting down on the cost of manufacturing. Fig. 18 shows the comparison of air-gap flux density distributions according to composition methods of cylindrical Halbach array using 3-D FEA. It can be seen that air-gap flux density due to parallel

magnetized arc segments makes little difference from it due to ideal radial magnetized PMs.

8.3 Thrust Measurement Results

Fig. 19 (b) reveals the comparison of analytical, FE and experimental results of axial thrust according to load current at mover position to create maximum thrust. As load current increases, experimental results become lower than analytical results owing to saturation of magnetic circuits.

9. Conclusion

In this paper, magnetic fields, thrust, flux linkages and back emf of the tubular linear actuator with Halbach and radial magnet array are presented. The analytical results have been verified by finite element analyses, confirming the worthiness of the proposed analysis. By presenting thrust characteristics according to such design parameters as magnet height and air-gap length, this paper predicted optimum design parameters so that PMs can be utilized efficiently. In particular, the tubular linear actuator with parallel magnetized arc segments is manufactured and experimental results such as thrust measurements are also given to confirm the analysis. The analytical model can be applicable to both slot and slotless topologies. In our future work, on the basis of analytical results, a dynamic analysis of a tubular linear actuator will be performed.

Acknowledgements

This work was financially supported by MOCIE through the IERC program, Korea.

References

[1] S. M. Jang, S. S. Jeong, "Armature Reaction Effect and Inductance of Moving Coil Linear Oscillatory Actuator with Unbalanced Magnetic Circuit", *IEEE Trans., Magn.*, vol. 37, pp. 2847-2850, July 2001.

[2] J. Wang, G.. W. Jewell, and D. Howe, "A general framework for the analysis and design of tubular linear permanent magnet machines", *IEEE Trans., Magn.*, vol. 35, pp. 1986-2000, 1999.

[3] Nicola Bianchi, "Analytical Computation of Magnetic Fields and Thrusts in a Tubular PM Linear Servo Motor", *IEEE Trans., Magn.*, vol. 1, pp. 21-28, 2000.

[4] Murray R. Spiegel, John Liu, "Mathematical Handbook of Formulas and Tables", Schaum's Outline Series, 2nd Edition, pp.152-153, 1999.

[5] Duane C. Hanselman, "Brushless Permanent-Magnet Motor Design", McGraw-Hill, pp. 70-71, 1994.

[6] Richard E. Clark, David Howe and Geraint W. Jewell, "The Influence of Magnetization Pattern on the Performance of a Cylindrical Moving-Magnet Linear Actuator", IEEE Trans., Magn., vol. 36, No. 5, pp. 3571-3574, Sept. 2000.

Seok-Myeong Jang

He was born in Korea in 1949. He received his B.E., M.S., and Ph.D. degrees from Hanyang University in 1976, 1978, and 1986, respectively. He is currently a Professor in the Department of Electrical Engineering, Chungnam National University. He worked as a Visiting Researcher in the Department of Electrical Engineering, Kentucky University in 1989. He is a member of KIEE. His field of interest includes the design and application of linear machines, high speed machines, and linear oscillating actuators.

Tel: +82-42-821-5658

Jang-Young Choi

He was born in Korea in 1976. He received his B.S. degree in Electrical Engineering from Chungnam National University in 2002. He is currently working toward his M.S. degree in the Dept. of Electrical Engineering at Chungnam National University. His research interests involve the design and analysis of linear machines.

Tel: +82-42-822-4933

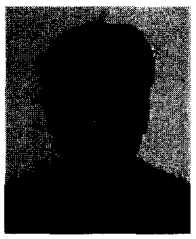

Sung-Ho Lee

He born in Korea in 1971. He received his B.S., M.S. and Ph.D. degrees in Electrical Engineering from Chungnam National University in 1997, 1999 and 2003, respectively. He has worked in the LG D/A Research Lab. His research interests include the design and analysis of linear machines and automatic electric machine performance monitoring.

Tel: +82-42-822- 4933

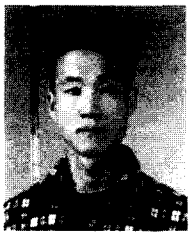

Han-Wook Cho

He was born in Korea in 1976. He received his B.S. degree in Electrical Engineering from Chungnam National University in 2002. He is currently working toward his M.S. degree in the Dept. of Electrical Engineering at Chungnam National University. His research interests involve the design and analysis of high speed machines.

Tel +82-42-822-4933

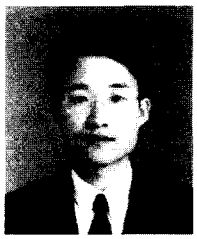

Won-Bum Jang

He was born in Korea in 1962. He received his B.S. and M.S. degrees in the Department of Electrical Engineering at Hanyang University in 1986 and 1988, respectively. He has worked in ADD. His research interests focus on the drive and dynamic simulation of linear machines.

Tel: +82-42-821-2670